Earthq Eng & Eng Vib (2008) 7:33-44 **DOI**: 10.1007/s11803-008-0825-8

Seismic response of bridge pier on rigid caisson foundation in soil stratum

C. Tsigginos[1†], N. Gerolymos[2‡], D. Assimaki[3§] and G. Gazetas[2*]

1. *National Technical University of Athens, Greece*
2. *Civil Engineering, National Technical University of Athens, Greece*
3. *Civil Engineering, Georgia Institute of Technology, Atlanta, USA*

Abstract: An analytical method to study the seismic response of a bridge pier supported on a rigid caisson foundation embedded in a deep soil stratum underlain by a homogeneous half space is developed. The method reproduces the kinematic and inertial responses, using translational and rotational distributed Winkler springs and dashpots to simulate the soil-caisson interaction. Closed-form solutions are given in the frequency domain for vertical harmonic S-wave excitation. Comparison with results from finite element (FE) analysis and other available solutions demonstrates the reliability of the model. Results from parametric studies are given for the kinematic and inertial responses. The modification of the fundamental period and damping ratio of the bridge due to soil-structure interaction is graphically illustrated.

Keywords: caisson; embedded foundations; kinematic response; inertial response; Winkler model; effective period; effective damping

1 Introduction

This article deals with the seismic response of a caisson-supported bridge pier, with a rectangular or square base. The soil is considered as a single homogeneous layer underlain by an elastic half space. The system is excited by vertical harmonic S-waves, specified through the "rock outcrop" motion. Analyses are performed in the frequency domain. The problem geometry is shown in Fig. 1.

Caisson foundations embedded in soft soil have been widely used to support major structures, especially bridges. In contrast to piles, which are relatively slender structural elements in lateral loading, caisson foundations are subjected to vertical shear tractions at their periphery and shear tractions at their base, in addition to the lateral soil reaction. Fig. 2 shows these tractions for a caisson with a rectangular cross section.

Correspondence to: George Gazetas, 36 Asimakopoulou Str., Ag. Paraskevi 15342, Greece
Fax: + 30 210 772 24 05
E-mail: gazetas@ath.forthnet.gr
†Civil Engineer; ‡Lecturer; §Assistant Professor; *Professor

Supported by: U.S. Federal Highway Administration Under Grant No. DTFH61-98-C-00094 and U.S. National Science Foundation Under Grant No. EEC-9701471
Received January 25, 2008; **Accepted** February 2, 2008

2 System and methods of analysis

2.1 Analysis model

The Winkler type model used for the solution of the problem is shown in Fig 3. The superstructure is modeled as a two degree-of-freedom (DOF) system, with a mass on the top of the column possessing rotational, in addition to translational, inertia. A complex modulus of elasticity simulates the damping in the structure.

To measure the soil reaction to displacement of the caisson, the dynamic Winkler multi-spring-and-dashpot model, developed by Assimaki (1998), Chantzigiannelis (1999) and Gerolymos & Gazetas (2007), is used. The model incorporates distributed translational (lateral) and rotational springs and dashpots along the caisson shaft, as well as concentrated translational (shear) and rotational (rocking) springs and dashpots at the base of the caisson. These four types of springs and dashpots are related to the resisting forces acting on the caisson shaft and base, as follows:

• The distributed lateral springs k_x and dashpots c_x are associated with the resulting horizontal soil reaction p_x on the circumference (shaft) of the caisson per unit depth:

$$p_x = (k_x + \mathrm{i}\omega c_x)\, u_x \tag{1}$$

• The distributed rotational springs k_θ and dashpots

c_θ are associated with the moment m_θ produced by the vertical shear tractions on the circumference of the caisson:

$$m_\theta = (k_\theta + \mathrm{i}\omega c_\theta)\,\theta_\mathrm{c} \tag{2}$$

• The resulting base shear translational spring K_x and dashpot C_x are associated with the horizontal shearing force on the base of the caisson:

$$Q = (K_x + \mathrm{i}\omega C_x)\,u_\mathrm{b} \tag{3}$$

• The resulting base spring K_θ and dashpot C_θ are associated with the moment produced by normal pressures on the base of the caisson:

$$M = (K_\theta + \mathrm{i}\omega C_\theta)\,\theta_\mathrm{c} \tag{4}$$

The dashpot coefficients reflect the combined radiation and hysteric "dissipation" of energy in the soil.

The elastic response of the bridge-foundation system is obtained by referring to the superposition theorem, along with decomposing the problem into kinematic and inertial responses (Whitman, 1972; Kausel & Roesset, 1974).

2.2 Response

The method of analysis is explained with the help of Fig. 4, for a perfectly rigid caisson of mass m_c and mass moment of inertia about its center of gravity J_c. The depth of embedment is D, while the thickness of the soil layer is H.

First, the response to S-waves of the free-field elastic soil layer over elastic bedrock is obtained from the well known equation (Kramer, 1996):

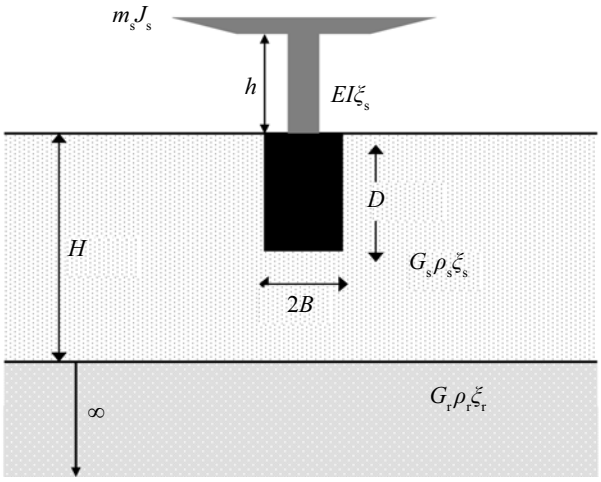

Fig. 1 The bridge caisson-soil system

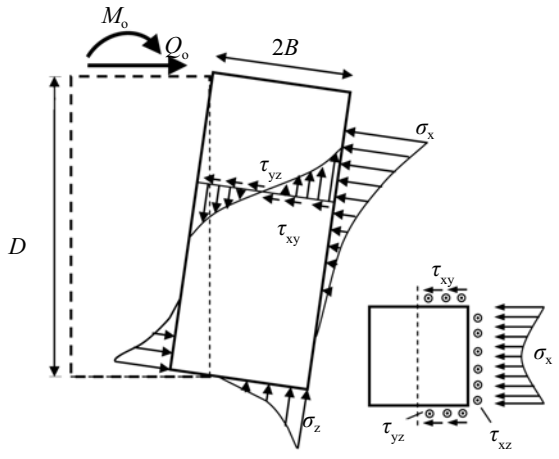

Fig. 2 Displacements of square caisson and mobilized soil reactions (Gerolymos&Gazetas, 2007; Assimaki *et al*., 2001)

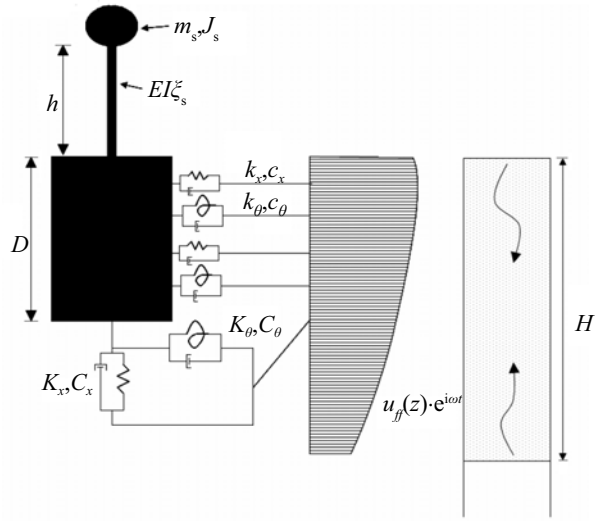

Fig. 3 The proposed model. The soil reactions are provided with four types of springs and dashpots, the mass is concentrated at the top of the pier, excited by the displacement profile of the 1-D computed free-field

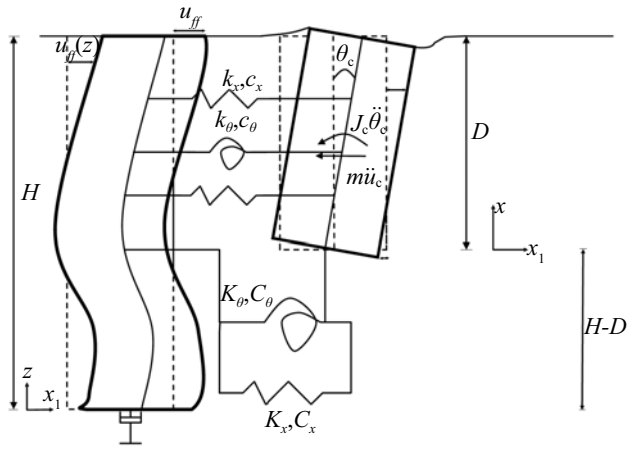

Fig. 4 Modeling of the kinematic interaction

$$u_{\mathrm{ff}}(z)=u_{\mathrm{g}}\frac{\exp\left[\mathrm{i}\kappa(H-z)\right]+\exp\left[-\mathrm{i}k(H-z)\right]}{(1+\alpha)\exp(\mathrm{i}kH)+(1-\alpha)\exp(-\mathrm{i}kH)} \tag{5}$$

where u_{g} is the amplitude of the harmonic displacement at the elastic rock, k is the complex wave number given by $k=\omega/V_{\mathrm{s}}\sqrt{1+2\mathrm{i}\xi_{\mathrm{s}}}$ and α is the complex soil-to-rock "*impedance ratio*":

$$\alpha=\frac{\rho_{\mathrm{s}}V_{\mathrm{s}}\sqrt{1+2\mathrm{i}\xi_{\mathrm{s}}}}{\rho_{\mathrm{r}}V_{\mathrm{r}}\sqrt{1+2\mathrm{i}\xi_{\mathrm{r}}}} \tag{6}$$

The caisson block performs a rigid-body steady-state oscillation when the supports of its interacting Winkler springs and dashpots are subjected to the free field motion given by Eq. (5). This motion is determined by the amplitude of displacement of the base u_{b} and the amplitude of rotation θ_{c}. At an arbitrary elevation z measured from the base, the caisson displacement equals $u_{\mathrm{b}}+\theta_{\mathrm{c}}z$.

The equations of dynamic equilibrium (horizontal translation and rotation) of the displaced caisson are written as:

$$\begin{aligned}&m_{\mathrm{c}}\ddot{u}_{\mathrm{c}}+\int_0^D k_x(x)(u(x,t)-u_{\mathrm{ff1}}(x,t))\mathrm{d}x+\\&\int_0^D c_x(x)(\dot{u}(x,t)-\dot{u}_{\mathrm{ff1}}(x,t))\mathrm{d}x+K_x(u_{\mathrm{b}}-u_{\mathrm{ff1}}(0,t))+\\&C_x(\dot{u}_{\mathrm{b}}-\dot{u}_{\mathrm{ff1}}(0,t))=0\end{aligned} \tag{7}$$

and

$$\begin{aligned}&J_{\mathrm{c}}\ddot{\theta}_{\mathrm{c}}+m_{\mathrm{c}}\ddot{u}_{\mathrm{c}}\frac{D}{2}+\int_0^D k_x(x)x(u(x,t)-u_{\mathrm{ff1}}(x,t))\mathrm{d}x+\\&\int_0^D k_\theta(x)(\theta(x,t)-\frac{\partial u_{\mathrm{ff1}}}{\partial x}(x,t))\mathrm{d}x+\int_0^D c_\theta(x)(\dot{\theta}(x,t)-\\&\frac{\partial^2 u_{\mathrm{ff1}}}{\partial x\partial t}(x,t))\mathrm{d}x+K_\theta(\theta_{\mathrm{b}}-\frac{\partial u_{\mathrm{ff1}}}{\partial x}(0,t))+\\&C_\theta(\dot{\theta}_{\mathrm{b}}-\frac{\partial^2 u_{\mathrm{ff1}}}{\partial x\partial t}(0,t))=0\end{aligned} \tag{8}$$

where

$$u_{\mathrm{ff1}}(x,t)=u_{\mathrm{ff}}[z-(H-D)] \tag{9}$$

and $u_{\mathrm{c}}=u_{\mathrm{c}}(t)$ is the displacement of the caisson at its center of gravity ($u_{\mathrm{c}}=u_{\mathrm{b}}+\theta_{\mathrm{c}}D/2$).

Taking $\ddot{u}=-\omega^2u$ and the form of the displacements of the caisson into consideration, Eqs. (7) and (8) can be written in the following matrix form

$$-\omega^2\boldsymbol{M}\begin{pmatrix}u_{\mathrm{b}}\\ \theta_{\mathrm{b}}\end{pmatrix}+\boldsymbol{K}\begin{pmatrix}u_{\mathrm{b}}\\ \theta_{\mathrm{b}}\end{pmatrix}=P \tag{10}$$

where the mass matrix is

$$\boldsymbol{M}=\begin{pmatrix}m_{\mathrm{c}} & m_{\mathrm{c}}\frac{D}{2}\\ m_{\mathrm{c}}\frac{D}{2} & m_{\mathrm{c}}\frac{D^2}{4}+J_{\mathrm{c}}\end{pmatrix} \tag{11}$$

The complex stiffness matrix is

$$\begin{aligned}\boldsymbol{K}&=\begin{pmatrix}\tilde{K}_x+\int_0^D\tilde{k}_x(x)\mathrm{d}x & \int_0^D\tilde{k}_x(x)x\mathrm{d}x\\ \int_0^D\tilde{k}_x(x)x\mathrm{d}x & \tilde{K}_\theta+\int_0^D\tilde{k}_x(x)x^2\mathrm{d}x+\int_0^D\tilde{k}_\theta(x)\mathrm{d}x\end{pmatrix}\\&=\begin{pmatrix}\tilde{K}_x+\tilde{k}_xD & \tilde{k}_x\frac{D^2}{2}\\ \tilde{k}_x\frac{D^2}{2} & \tilde{K}_\theta+\tilde{k}_\theta D+\frac{1}{3}\tilde{k}_xD^3\end{pmatrix}\end{aligned} \tag{12}$$

where, $\tilde{\boldsymbol{K}}=\boldsymbol{K}+\mathrm{i}\omega\boldsymbol{C}$, and $\boldsymbol{P}$ is the vector of effective loading

$$\boldsymbol{P}=\begin{pmatrix}\int_0^D\tilde{k}_x(x)u_{\mathrm{ff1}}(x)\mathrm{d}x+\tilde{K}_xu_{\mathrm{ff1}}(0)\\ \int_0^D\tilde{k}_\theta(x)u'_{\mathrm{ff1}}(x)\mathrm{d}x+\int_0^D\tilde{k}_x(x)xu'_{\mathrm{ff1}}(x)\mathrm{d}x+\tilde{K}_\theta u'_{\mathrm{ff1}}(0)\end{pmatrix} \tag{13}$$

The dynamic impedance matrix $\boldsymbol{S}$ at the top of the caisson, obtained by a coordinate transformation, is given by

$$\tilde{\boldsymbol{S}}=\begin{pmatrix}\tilde{S}_x & \tilde{S}_{x\theta}\\ \tilde{S}_{x\theta} & \tilde{S}_{\theta\theta}\end{pmatrix}=\begin{pmatrix}\tilde{K}_{xx} & \tilde{K}_{x\theta}-D\tilde{K}_{xx}\\ \tilde{K}_{xr}-D\tilde{K}_{xx} & \tilde{K}_{\theta\theta}-2D\tilde{K}_{x\theta}+D^2\tilde{K}_{xx}\end{pmatrix} \tag{14}$$

where $\tilde{K}_{xx},\tilde{K}_{x\theta},\tilde{K}_{\theta\theta}$ are the elements of the stiffness matrix of Eq. (12).

In the same way, the mass matrix of the top of the caisson is given by the following equation

$$\tilde{\boldsymbol{M}}=\begin{pmatrix}m_{\mathrm{c}} & -m_{\mathrm{c}}\frac{D}{2}\\ -m_{\mathrm{c}}\frac{D}{2} & J_{\mathrm{c}}+m_{\mathrm{c}}\frac{D^2}{4}\end{pmatrix} \tag{15}$$

2.3 Inertial and total response

The method of analysis (Mylonakis *et al.*, 1997) is schematically illustrated in Fig 5. As previously mentioned, the mass of the superstructure is concentrated at the top of the pier, and the pier is modeled as a beam. The soil-caisson interaction is reproduced through the dynamic impedances computed in the previous subsection.

For the steady-state harmonic response in the frequency domain, the differential equations of motion reduce to:

$$\left(\begin{bmatrix} \boldsymbol{K}_{ss} & \boldsymbol{K}_{sb} \\ \boldsymbol{K}_{bs} & \boldsymbol{K}_{bb}+\boldsymbol{S}_{ij} \end{bmatrix} - \omega^2 \begin{bmatrix} \boldsymbol{M}_{ss} & \boldsymbol{M}_{sb} \\ \boldsymbol{M}_{bs} & \boldsymbol{M}_{bb} \end{bmatrix}\right) \begin{Bmatrix} u_{tot} \\ \theta_{tot} \\ u_b \\ \theta_b \end{Bmatrix} = \begin{Bmatrix} 0 \\ 0 \\ \boldsymbol{S}_{ij} \begin{Bmatrix} u_{kin} \\ \theta_{kin} \end{Bmatrix} \end{Bmatrix} \tag{16}$$

where $\boldsymbol{K}_{ss}$, $\boldsymbol{K}_{sb}$, $\boldsymbol{K}_{bs}$ and $\boldsymbol{K}_{bb}$ are the four stiffness submatrices corresponding to the superstructure and the foundation; $\boldsymbol{m}_{ss}$, $\boldsymbol{m}_{sb}$, $\boldsymbol{m}_{bs}$ and $\boldsymbol{m}_{bb}$ are the relevant mass submatrices.

3 Calibration of springs and dashpots

Evidently, the reliability of the method depends on a proper choice of the dynamic spring and dashpot "constants" as function of frequency.

Analytical expressions for these "constants" were obtained by calibrating the model against the closed-form expressions presented by Gazetas (1991) for rectangular foundations of L/B = 1-6, embedded in a homogeneous half space at depth $D \leq 2B$, as depicted in Fig 6. These expressions had been based on the results of rigorous boundary-element and finite-element elastodynamic analysis, as well as on other available solutions from the literature. For a rectangle of width $2B$ and length $2L$ ($L > B$) in a homogeneous half space, the dynamic impedances are expressed (with respect to the center of the base mat) in the form

$$\tilde{\boldsymbol{K}}_{emb} = \boldsymbol{K}_{emb}\chi_{emb}(\omega) + i\omega \boldsymbol{C}(\omega) \tag{17}$$

where $\boldsymbol{K}_{emb}$ is the static stiffness of the embedded foundation and $\chi_{emb}(\omega)$ is frequency dependent dynamic stiffness coefficient. $\boldsymbol{C}(\omega)$ is the frequency dependent damping coefficient (encompassing both the radiation and the material damping of the system). The parameters which enter in the springs and dashpots are:

- G_s, V_s, V_{La} and ν denote, respectively, the shear modulus of elasticity, the shear wave velocity, the apparent propagation velocity of compression-extension waves, and Poisson's ratio of the soil.
- B, L and D denote, respectively, the semi-width, the semi-length and depth of the embedment.

Gazetas and Tasoulas (1987a) developed the following expression for the horizontal static stiffness in the longitudinal (x)-axis of an orthogonal caisson embedded in a homogeneous soil:

$$\boldsymbol{K}_{xx}(\omega) = \left\{\frac{2G_sL}{2-\nu}\left(2+2.5\left(\frac{4BL}{4L^2}\right)^{0.85}\right) - \frac{0.2}{0.75-\nu}G_sL\left(1-\frac{B}{L}\right)\right\} \left(1+0.15\sqrt{\frac{D}{B}}(1+0.52\left(\frac{4(B+L)D^2}{3BL^2}\right)^{0.4}\right) \tag{18}$$

The dynamic coefficient χ_{emb} is presented in chart form

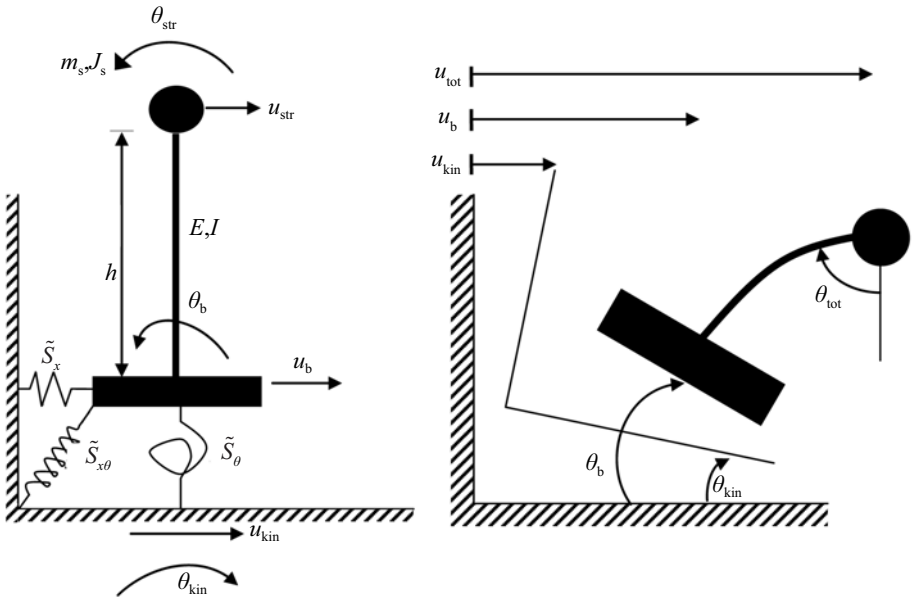

Fig. 5 Analysis model for the inertial interaction. the model parameters (left) and the response (right) in terms of absolute displacements and rotations

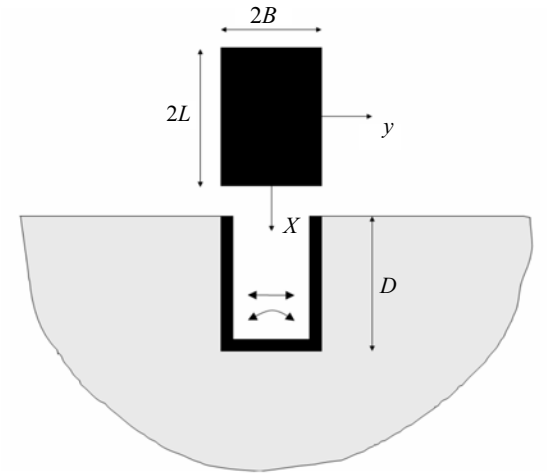

Fig. 6 Geometry of a rigid orthogonal foundation embedded in a homogeneous elastic half space

(Gazetas and Tasoulas, 1987a) in terms of D/B and L/B as a function of the dimensionless parameter $a_0(=\omega b/V_s)$.

For a square caisson, the dynamic stiffness coefficient $\chi_{emb}(\omega)$ is given by the following equation

$$\chi_{\text{emb}}(\omega) \approx 1+\alpha_0\left(\frac{D}{2B}\right)\left\{\left[0.08-0.0074\left(\frac{D}{2B}\right)\right]\alpha_0{}^2 - \left[0.31-0.0416\left(\frac{D}{2B}\right)\right]\alpha_0 - 0.0442\left(\frac{D}{2B}\right)+0.14\right\} \quad (19)$$

The corresponding static rocking stiffness (Gazetas, 1991) is

$$K_{\theta\theta}(\omega)=\frac{G_s}{1-\nu}\left(\frac{16BL^3}{12}\right)^{0.75}\left(3\left(\frac{L}{B}\right)^{0.15}\right)\left\{1+0.92\left(\frac{D}{L}\right)^{0.6}\left[1.5+\left(\frac{D}{L}\right)^{1.9}\right]\right\} \quad (20)$$

The dynamic stiffness:

$$\chi_{\theta,\text{emb}} \approx 1 - 0.3\alpha_0 \quad (21)$$

The dashpots are given by the following general expression

$$C_{\text{tot}} = C_{\text{radiation}} + 2\xi K \quad (22)$$

For the horizontal translational, the radiation dashpot coefficient (Gazetas and Tasoulas, 1987b) is

$$C_{xx} = 4\rho V_s BLc_x + 4\rho V_s LD + 4\rho V_{\text{La}} DB \quad (23)$$

where c_h is given in chart form in Gazetas (1991)

In rocking oscillation, the radiation damping (Fotopoulou *et al.*, 1989) is expressed as

$$C_{\theta\theta} = \frac{4}{3}\rho V_{\text{La}} L^3 Bc_{\theta\text{b}}(\omega) + \frac{4}{3}\rho V_{\text{La}} D^3 Bc_1 + \frac{4}{3}\rho V_s LD(L^2+D^2)c_1 + 4\rho V_s L^2 DBc_1 \quad (24)$$

where $c_{\theta b}$ is

$$c_{\theta\text{b}} \approx \{-0.07 + 0.0001\left(\frac{L}{B}\right)^2\} + \{1 - 1.22(0.55)^{L/B}\}\left(\frac{\omega B}{V_s}\right)^{L/B} \quad (25)$$

And c_1 is

$$c_1 \approx 0.25 + 0.65\sqrt{\frac{\omega B}{V_s}}\left(\frac{D}{B}\right)^{-0.25} \quad (26)$$

The non-diagonal terms of the complex stiffness matrix is

$$\tilde{K}_{x\theta} \approx \frac{1}{3}D\tilde{K}_{\theta\theta} \quad (27)$$

Thus, the stiffness matrix of the caisson at the base of the caisson has been calculated as

$$\tilde{\boldsymbol{K}}_{\text{emb}} = \begin{pmatrix} \tilde{K}_{\text{xx}} & \tilde{K}_{x\theta} \\ \tilde{K}_{x\theta} & \tilde{K}_{\theta\theta} \end{pmatrix} \quad (28)$$

To determine the distributed springs and dashpots, the diagonal terms of the matrices in Eqs. (28) and (12) are equated as

$$\tilde{k}_x = (\tilde{K}_{xx} - \tilde{K}_x)/D \quad (29)$$

$$\tilde{k}_\theta = \left(\tilde{K}_{\theta\theta} - \tilde{K}_\theta + \frac{1}{3}D^2\tilde{K}_x - \frac{1}{3}D^2\tilde{K}_{\theta\theta}\right)/D \quad (30)$$

For a square caisson and an orthogonal caisson with L/B=2 and static lateral loading, the distributed springs are

Square caisson

$$k_x \approx 2.1\left(\frac{D}{B}\right)^{-0.14}E_s \quad \text{and} \quad k_\theta \approx 4\left(\frac{D}{B}\right)^{-1.5}E_s D^2 \quad (31)$$

Orthogonal caisson L/B=2

$$k_x \approx 2\left(\frac{D}{B}\right)^{-0.16}E_s \quad \text{and} \quad k_\theta \approx 11\left(\frac{D}{B}\right)^{-2}E_s D^2 \quad (32)$$

For the case of an elastic soil layer underlain by a homogeneous half space, the base coefficient (for

horizontal translation and rotation) is

$$K_{\text{broel}} = K_{\text{homstat}} \cdot k\left(\frac{L}{B},\frac{H}{B},\frac{G_{\text{s}}}{G_{\text{r}}}\right)\cdot \chi_{\text{roel}}\left(\frac{G_{\text{s}}}{G_{\text{r}}},\frac{H}{B},\frac{L}{B},\omega\right) \tag{33}$$

where, the factor k models the different "pressure bulb" under static loading.

Based on results of circular and strip foundations (Gazetas, 1983), the following two equations for the factor k can be derived, using an equivalent circular foundation for a square foundation.

$$k_x = \frac{\left(1+\left(1+0.5+\frac{B}{L}\right)^{-1}\right)\frac{B}{H}}{\left(1+\left(1+0.5+\frac{B}{L}\right)^{-1}\right)\frac{B}{H}\frac{G_{\text{s}}}{G_{\text{r}}}} \tag{34}$$

and

$$k_\theta = \frac{1+\left(1/(5+\frac{B}{L})\right)\frac{B}{H}}{1+\left(1/(5+\frac{B}{L})\right)\frac{G_{\text{s}}}{G_{\text{r}}}} \tag{35}$$

And χ_{roel} is given in Gazetas (1991) in chart form in terms of L/B and H/B as a function of a_0.

Taking Eq. (33) into account, the diagonal terms of the stiffness matrix are:

$$K_{xx\text{roel}} = K_{x\text{broel}} + k_x D \tag{36}$$

$$K_{\theta\theta\text{roel}} = K_{\theta\text{broel}} + k_x D + \frac{1}{3}k_x D \tag{37}$$

A cut-off frequency exists (for radiation damping) in this case. To simulate this phenomenon, the method of linear interpolation is used. For frequencies smaller than (4/3) f_{s}, the radiation damping coefficients are zero. For frequencies greater than 1.33 f_{s}, the damping coefficients of the homogeneous half space are used. For intermediate values, linear interpolation is used.

$$\tilde{c}_{\text{rock}} = \begin{cases} 0, & \omega \le \frac{3}{4}\frac{7\pi V_{\text{s}}}{2H} \\ \frac{24cH}{7\pi V_{\text{s}}}\omega - \frac{9c}{7}, & \frac{3}{4}\frac{\pi V_{\text{s}}}{2H} \le \omega \le \frac{4}{3}\frac{\pi V_{\text{s}}}{2H} \\ c_{\text{hom}}, & \omega \ge \frac{4}{3}\frac{\pi V_{\text{s}}}{2H} \end{cases} \tag{38}$$

where c is the radiation damping for $\omega = 1.33\pi V_{\text{s}}/(2H)$. The linear interpolation method must be used only in the inertia response step.

4 Comparison with 3D finite-element (FE) analysis and other solutions

To evaluate the accuracy of the proposed model, a comparison is performed between results from finite-element method (FEM) analysis, and other solutions from the literature. The geometry used in the FEMs is depicted in Fig. 7.

The problem studied with the FEM is a rigid caisson with $2B$=4m, D/B=4 or 6, and H/B=10m. Shear modulus and mass density are constant with depth: G=50000kPa, v=0.3, and ρ_{s}=1.8mg/m^3. The following numerical model is developed with ABAQUS. Both the caisson and the soil are modelled with 3D elements. The mass of the superstructure is assumed to be lumped at the top of the pier. The elastic bedrock is modelled with dashpots. The side boundaries are assumed to be free, thus above the cut-off frequency. A different radiation, compared to the conditions of the proposed model, will occur due to the reflections in the side boundaries. For the kinematic response, Rayleigh damping is used (constant and equal to 0.05 at the first two modes) and an elastic model (ξ=0%) is assumed for the inertia response.

In Fig. 8, the proposed model for the kinematic interaction is compared to a solution given by the FEM. According to Fig (9), there is a good correlation in the first two modes. This has occurred for the following three reasons. Firstly, the springs and dashpots, which are used to calibrate the model, are developed in a region of 0-2 for the dimensionless frequency a_0. Secondly, the damping in the FE model is not-constant for all the eigenmodes. Finally, the different boundary conditions for the side boundaries in the two models; in the proposed Winkler-model, these boundaries are extended

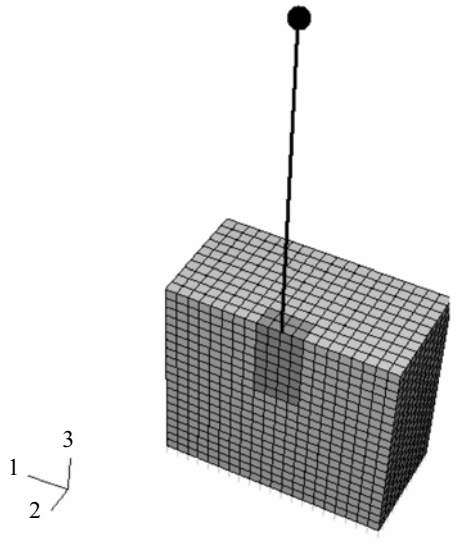

Fig. 7 An intersection of the finite element model. The caisson and beam elements are shown with deep grey colour, the surrounding soil with soft grey. The elastic rock halfspace is simulated with dashpots

to infinity but in the FEM model, they are very close to the caisson (the whole model is a 20m×20m×20m box).

In Fig. 9 the proposed model for the inertia interaction is compared with a solution given by the FEM. Note that there is a good correlation for the period of the system.

Finally, the eigenperiod, which is taken from the model, is compared with the solution given by Veletsos (1977) and Bielak (1975) as shown in Fig. 10. The dimensionless parameters given in these figures are explained in the following section.

5 Results of parametric studies

5.1 Kinematic interaction

While long piles follow more or less the seismic motion of the ground, a rigid caisson substantially modifies the soil deformation. As a result, the incident seismic waves are scattered and the seismic excitation to which the caisson is effectively subjected may differ considerably from the free field motion. To present the analysis results, the following dimensionless parameters are defined:

• the 'effective' displacement ratio at the top of the caisson

$$\eta_{\text{eff}}(\omega)=\frac{u_{\text{kin}}(\omega)}{u_{\text{ff}}(H,\omega)} \tag{39}$$

• the 'effective' rotation at the top of the caisson

$$\theta_{\text{eff}}(\omega)=\frac{\theta_{\text{kin}}(\omega)D}{u_{\text{ff}}(H,\omega)} \tag{40}$$

• the amplification ratio at the top of the soil layer

$$A_{\text{ff}}(\omega)=u_{\text{ff}}(H,\omega)\,/\,u_{\text{ff}}(0,\omega) \tag{41}$$

• the amplification at the top of the caisson

$$A_{\text{cc}}(\omega)=u_{\text{kin}}(\omega)\,/\,u_{\text{ff}}(0,\omega) \tag{42}$$

Two dimensionless frequency parameters facilitate the presentation of results: $c_0=\omega H/V_s$ is a parameter with respect to the thickness of the deposit, and $\beta_0=\omega D/V_s$ is a parameter with respect to the depth of embedment. It has been proven that the response is governed for each frequency by the following two parameters: the soil layer depth to the depth of embedment ratio H/D and the shear modulus ratio G_s/G_r.

Figure 11 shows the influence of the first parameter upon the behavior of the caisson. Apparently, the deep caissons do not follow the soil motion at higher frequencies.

Finally, Figs. 12(a) and (b) show the variation of the η_{eff} and the θ_{eff} with dimensionless frequency (β_0), respectively.

5.2 Inertia interaction

The effective period of the system is controlled by the following three dimensionless parameters:

(1) Slenderness ratio, h/B

(2) Ratio of masses of the bridge and the caisson, $\boldsymbol{m_{\text{str}}/m_{\text{c}}}$

(3) Relative stiffness of the fixed base structure and the soil, $\omega_{\text{str}}h/V_s$

Figure 13 shows the influence of the slenderness ratio on the effective period of the system. For small slenderness ratios, the effective period has a greater increase than for higher slenderness ratios. This can be

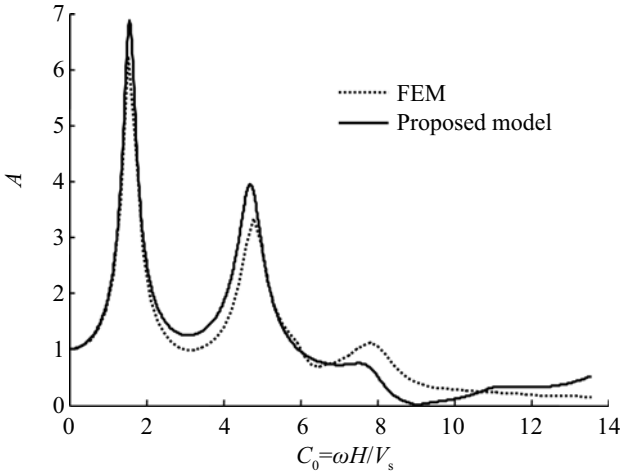

Fig. 8 Comparison of amplification factors from the proposed model & solutions of FEM for kimematic interaction (α=0.085, ξ=0.05, *D/B*=6, *H/B*=20)

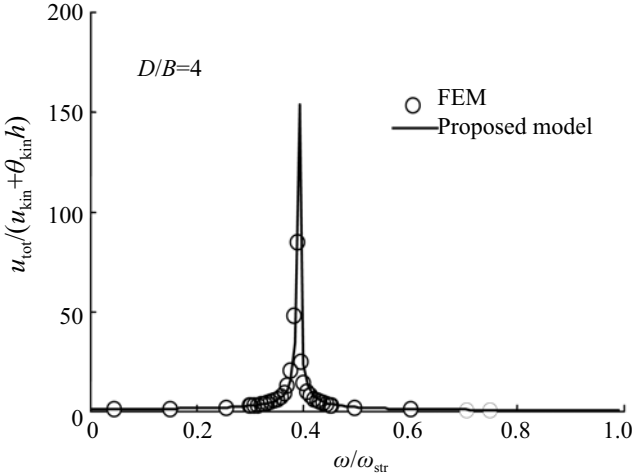

Fig. 9 Inertia interaction: comparison with FE solution. (*G*=50MPa, α=0.085, *B*=2m, *E*=30GPa, I_x=64m^4, m_{str}=1200Mg, *h*=30m)

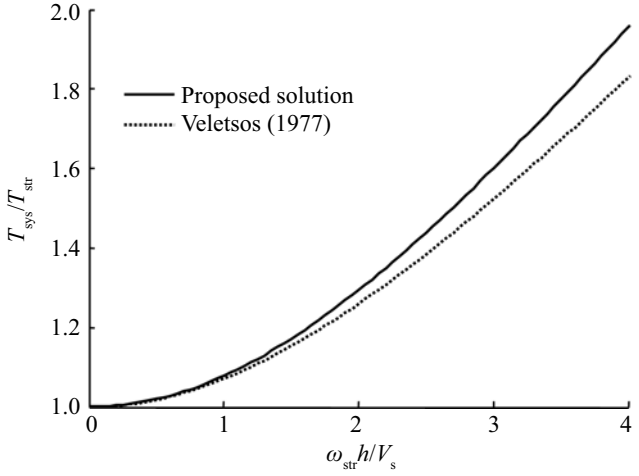

Fig. 10 Comparison of the structure periods from the proposed model & that proposed by Veletsos (1977), (m_{str} / m_c=0.28, h/b =4)

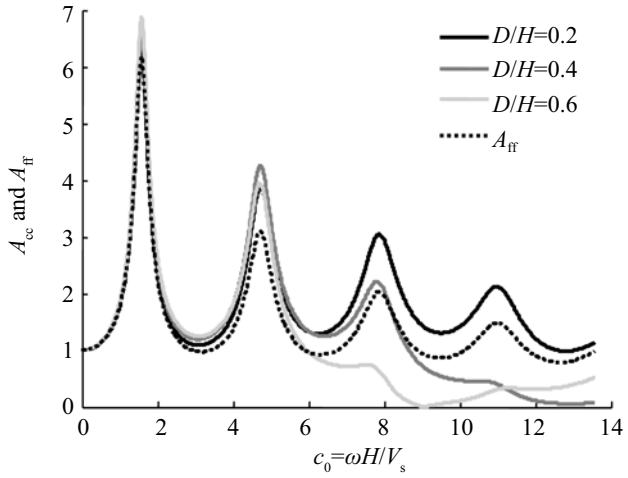

Fig. 11 Comparison of the transfer functions between top (z=H) and base (z=0) displacement amplitudes, for the free filed (A_{ff}) and the caisson (A_{cc}). Square caisson with D/H=0.2, 0.4 and 0.6.(α = 0.08, ξ_s = 0.05)

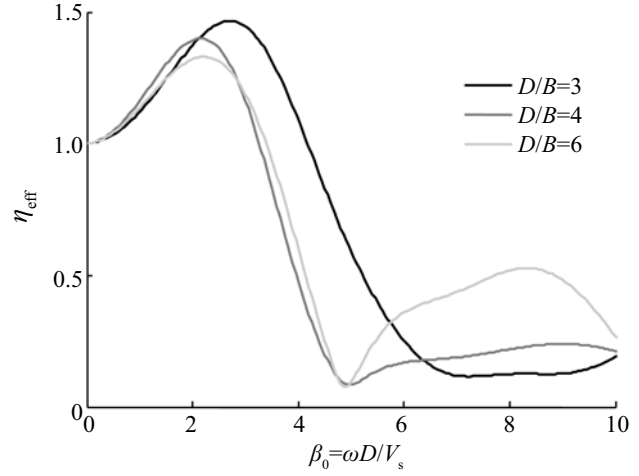

(a) Normalized 'effective' displacement of the top of the caisson

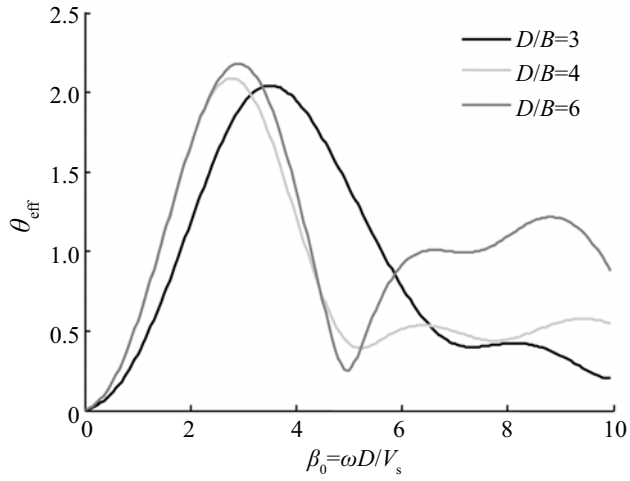

(b) Normalized 'effective' rotation of the caisson

Fig. 12 Variation of η_{eff} and θ_{eff} with dimensionless frequency β_0 for square caisson with slenderness ratio D/B=3,4, and 6.(α = 0.083, D/H = 0.16)

explained by the fact that in tall, slender structures, the predominant displacement is the rotation against which a caisson behaves very rigidly.

Figure 14 shows the influence of the ratio of the masses. The effective period of the system increases monotonically with the mass ratio. When the ratio tends to zero, the mass of the caisson is very big compared to the mass of the bridge, thus the superstructure acts as if it is founded on a fixed base.

Figure 15 shows the influence of the term $\omega_{str}h/V_s$ on the effective period of the system. As the ratio increases (the structure may be based on a soft soil), the period also increases.

The following equation is proposed for the effective period of the system compared to the fixed-base period of the superstructure.

$$\frac{\tilde{T}_{sys}}{T_{str}} \approx 1+\left(\frac{h}{B}\right)^{-0.5}\left(\frac{m_{str}}{m_c}\right)^{0.613}\left(\frac{h\omega_{str}}{V_s}\right)^{1.18} \tag{43}$$

The damping ratio encompasses the hysteric damping in the soil, the radiation damping and the structural damping.

The frequency of the system is given by the following equation

$$\omega_{sys,dam} = \frac{\omega_{sys}}{\sqrt{1-\xi^2}} \tag{44}$$

and

$$A = \frac{1}{2\xi\sqrt{1-\xi^2}} \tag{45}$$

Solving Eq. (45) for ξ, one obtains

$$\xi = \frac{\sqrt{1-\frac{\sqrt{A^2-1}}{A}}}{\sqrt{2}} \tag{46}$$

where A is defined as

$$A = \frac{u_{\text{str}}}{u_{\text{kin}} + h\theta_{\text{kin}}} \tag{47}$$

The results, which follow, are given for a constant hysteric damping equal to 5% for both the soil and the structure.

Three different types of soil are examined. The first two soil cases are extreme conditions, where the cut-off frequency tends to zero and infinity, respectively.

The influence of the slenderness ratio on the damping ratio for two different soil conditions is shown in Fig. 16. For tall, slender structures, the damping ratio is equal to the structural damping ratio, and for structures with a ratio h/B<10, the damping ratio increases. This can be explained by the fact that tall and slender structures are more prone to structural deformation and rotation than to lateral caisson displacement.

Figure 17 shows the influence of the mass ratio on the effective damping. As the mass ratio decreases, the periphery of the caisson increases, thus more seismic waves are emitted from the periphery. Therefore, the radiation damping plays a significant role in the behavior of the superstructure.

Figure 18 gives the influence of the term $\omega_{\text{str}}h/V_{\text{s}}$ on the effective damping. As the ratio increases, the damping ratio also increases. Note that large values of the relative stiffness are related to soft soils.

Finally, the influence of D/B on the damping ratio

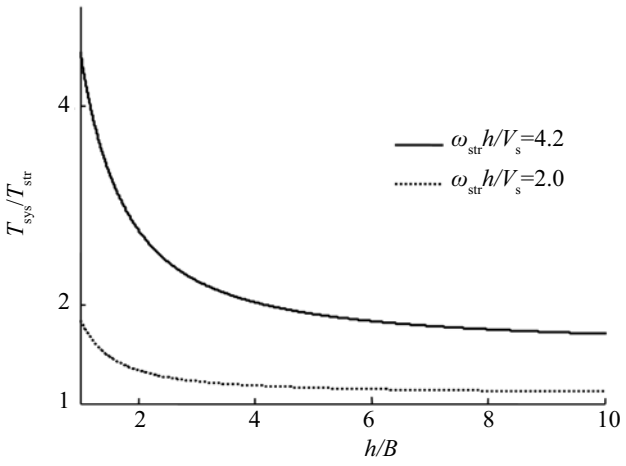

Fig. 13 Effect of slenderness ratio on the effective period of the system (J_{s}=0, $m_{\text{str}}/m_{\text{c}}$=4.2)

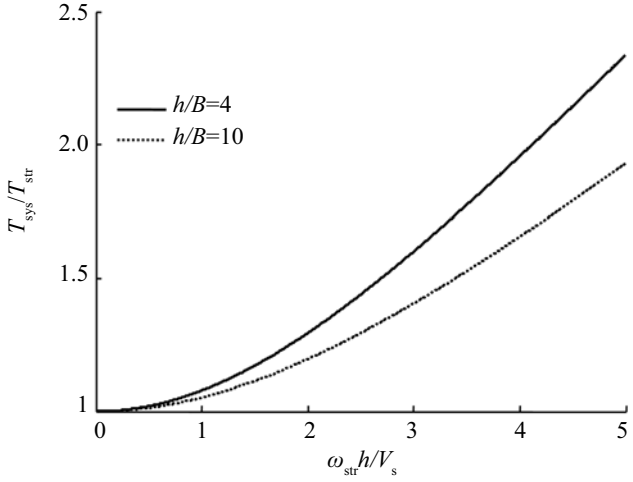

Fig. 15 Effect of the relative stiffness of soil and structure, $\omega_{\text{str}}h/V_{\text{s}}$, on the effective period of the system

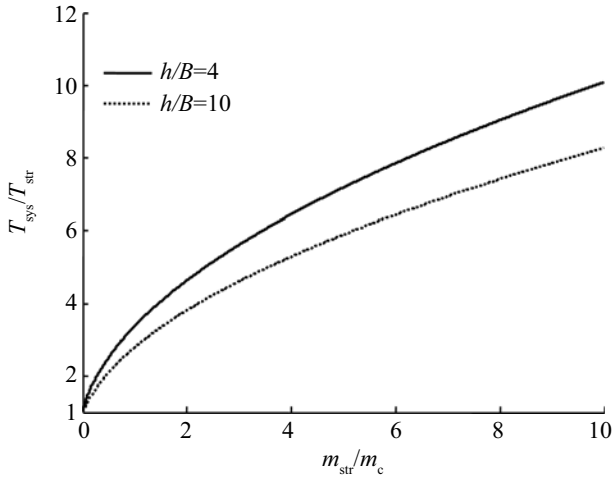

Fig. 14 Effect of the relative mass ratio on the effective period of the system. (J_{s}=0, $\omega_{\text{str}}h/V_{\text{s}}$=4.2)

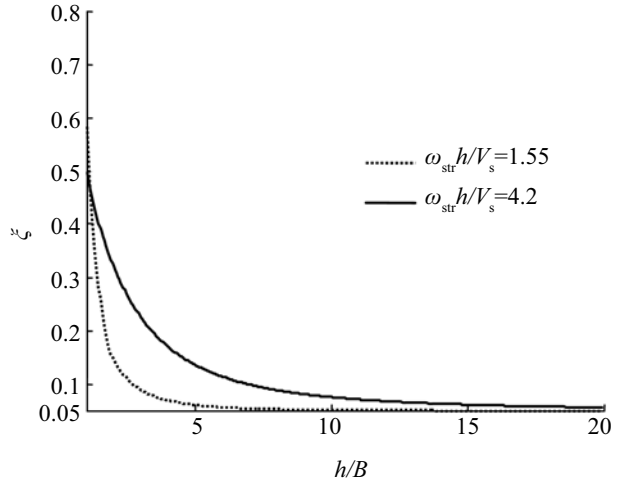

Fig. 16 Effect of the slenderness ratio on the total damping (radiation plus hysteric and structural damping) for two different soils (J_{s}=0, m_{str} / m_{c} =0.28, D/B=4)

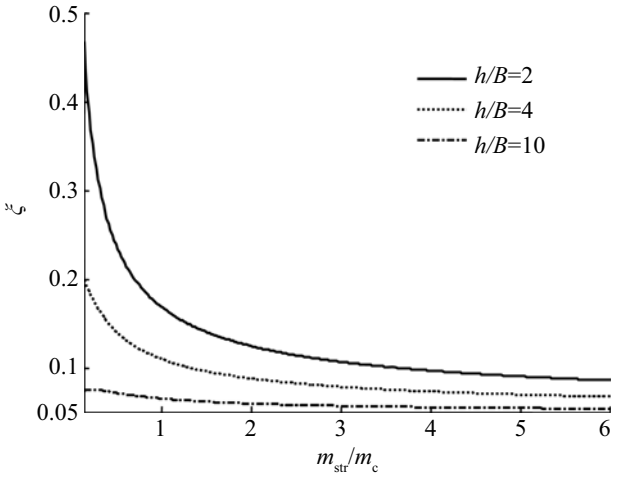

Fig. 17 The effect of the relative mass ratio on the total damping, radiation plus hysteric and structural damping, for three different slenderness ratio. (J_s=0, $\omega_{str}h/V_s$=4.2, D/B=4)

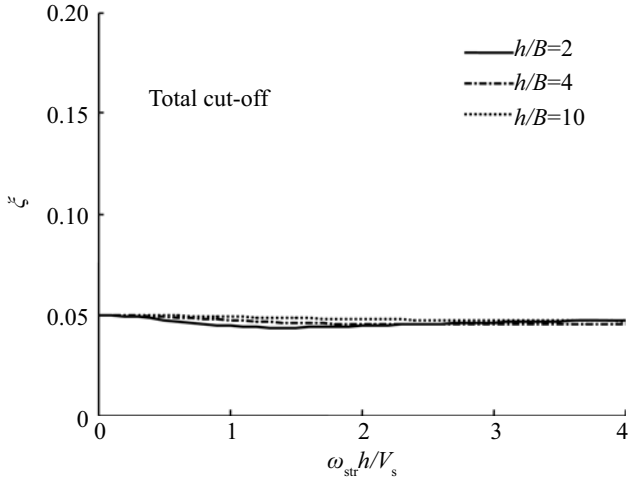

Fig. 20 The effective damping for a soil with total cut-off conditions ($f<f_c$). The effective damping is approximately the structural damping.(m_{str} / m_c = 0.28, D/B=2)

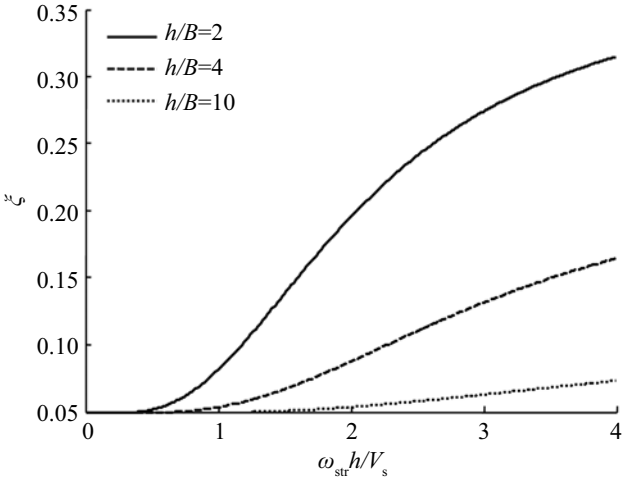

Fig. 18 The effect of the relative stiffness of the soil and the structure, on the effective damping, for three different slenderness ratios. (J_s=0, m_{str} / m_c =0.28, D/B=4)

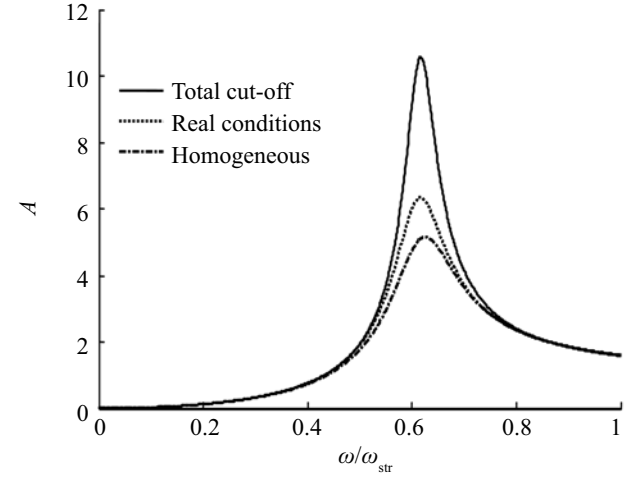

Fig. 21 The importance of different amounts of radiation damping on the resonant peak.($\omega_{str}h$ / V_s=1.75, m_{str}/m_c=0.82, h/B=5, D/B=4)

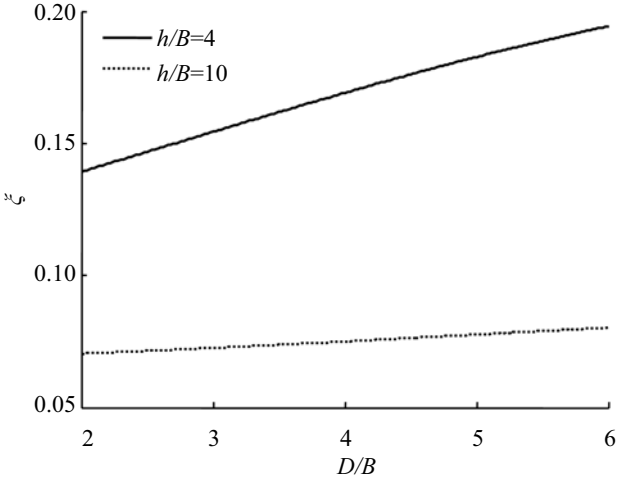

Fig. 19 The effect of the D/B on the total damping,radiation plus hysterical and structural damping, for two different slenderness ratios.($\omega_{str}h/V_s$=4.2, m_{str}/ m_c = 0.277)

is given in Fig. 19. As the D/B increases, the damping ratio increases. This can be explained by the fact that increasing this ratio under a constant relative mass ratio, the perimeter of the caisson also increases, which leads to an increase of the radiation damping.

The effective damping for soils in total cut-off conditions is approximately the same as the structure damping, as shown in Fig. 20.

Figure 21 shows the importance of radiation damping in the behavior of the system.

In the final type of soil, there are three distinct regions for the radiation damping:

- When $\omega_{sys}/\omega_{soil} < 0.8$, no radiation damping develops,
- When $\omega_{sys}/\omega_{soil} > 1.2$, the full radiation damping of the homogeneous half space develops, and
- When $0.8 < \omega_{sys}/\omega_{soil} < 1.2$, radiation damping takes intermediate values.

6 Conclusions

An analytical method to study the seismic response of a bridge pier supported on a rigid caisson foundation embedded in a deep soil stratum is developed. The method reproduces the kinematic and inertial response. Closed-form solutions are given in the frequency domain for vertical harmonic S-wave excitation. From the comparison with results from finite element (FE) analysis and other available solutions, the reliability of the proposed model is verified and the following conclusions can be drawn.

(1) The proposed model yields satisfactorily results in the first and second eigenmodes; in other words, for values of dimensionless frequency a_0 less than 2.

(2) The modification of the seismic waves is more intense in caissons with small values of the soil layer depth and the caisson embedment depth ratio H/D.

(3) The increase of the period of the structure due to soil-caisson-structure interaction is controlled by the slenderness ratio, the relative masses and the relative stiffness of the structure and the soil, and the increase can be very significant for stiff structures with small values of the slenderness ratio. Even for flexible structures with the slenderness ratio greater than ten founded in soft soils, the period of the system can be increased by 50%.

(4) The increase of the damping ratio of the system is due to the radiation damping. Specifically, this increase is controlled by the slenderness ratio, the relative masses, the relative stiffness of the structure in a fixed base condition and the soil, and the depth of embedment. The most important parameter is the slenderness ratio, because for high values of this ratio, the radiation damping tends to be zero. Furthermore, a relatively large mass of the caisson compared to the mass of the superstructure leads to an increase in the radiation damping.

In the case of a 'real' soil layer with a depth of H, the period of the system influences its damping ratio. If the period of the system is smaller than the period of the soil layer, the damping ratio will be the damping of the homogenous soil condition. Conversely, if the period of the soil layer is smaller than the period of the structure, the damping ratio will be equal to the structural damping.

References

Assimaki D (1998), "Static and Dynamic Analysis of Caissons Subjected to Lateral and Static Loading," *Diploma Thesis*, N.T.U.A, Athens. (in Greek)

Assimaki D, Chatzigiannelis I, Gerolymos N and Gazetas G (2001), "Lateral Response of Caissons Foundations," *Proc 4th National Conference on Geotechnical and Geoenvironmental Engineering*, Athens, Greece, June. (in Greek)

Bielak J (1975), "Dynamic Behavior of Structures with Embedded Foundations," *Earthquake Engineering and Structural Dynamics*, **3**: 259-274.

Chatzigiannelis I (1999), "Lateral Static and Dynamic Analysis of Caissons in Non Homogeneous-Halfspace," *Diploma Thesis*, N.T.U.A, Athens. (in Greek)

Fotopoulou M, Konstantopoulos P, Gazetas G and Tassoulas JL (1989), "Rocking Damping of Arbitrarily-shaped Embedded Foundations," *Journal of Geotechnical Engineering*, ASCE, **115**(4): 473-489.

Gazetas G (1983), "Analysis of Machine Foundation Vibrations: State of the Art," *Soil Dynamics and Earthquake Engineering,* **2**(1): 2-42.

Gazetas G (1991), "Formulas and Charts for Impendances of Surface and Embedded Foundations," *Journal of Geotechnical Engineering,* ASCE, **117**(9): 1363-1381.

Gazetas G and Tasoulas J (1987a), "Horizontal Stiffness of Arbitrarily Shaped Embedded Foundations," *Journal of Geotechnical Engineering,* ASCE, **113**(5): 440-457.

Gazetas G and Tasoulas J (1987b), "Horizontal Damping of Arbitrarily Shaped Embedded Foundations," *Journal of Geotechnical Engineering,* ASCE, **113**(5): 458-475.

Gerolymos N and Gazetas G (2007), "Winkler Model for Lateral Response of Rigid Caisson Foundations in Linear Soil," *Soil Dynamics and Earthquake Engineering,* **26**: 347-361.

Gerolymos N, Gazetas G and Mylonakis G (1998), "Foundemental Period and Effective Damping of Pile-supported Bridge Piers", *11th European Conference on Earthquake Engineering,* Topic 3.

Kausel E and Roesset JM (1974), "Soil-structure Interaction for Nuclear Containment Structures," *Proceedings. ASCE, Power Division Specialty Conference,* Boulder, Colorado.

Kramer S (1996), "Geotechnical Earthquake Engineering," EngleWood Cliffs: Prentice Hall.

Mylonakis G (2001), "Elastodynamic Model for Large Diameter End-bearing Shafts," *Soil Foundations,* **41**(3): 31-44.

Mylonakis G, Nikolaou A and Gazetas G (1997), "Soil-pile-bridge Seismic Interaction: Kinematic and Inertial Effects, Part I: Soft Soil," *Earthquake Engineering and Structural Dynamics,* **26**: 337-359.

Veletsos AS (1977), "Dynamics of Structure Foundation Systems," *Structural and Geotechnical Mechanics, N.M. Newmark Honoring Volume*, Prentice Hall, pp 333-361.

Whitman RV (1972), "Analysis of Soil-structure Interaction: State-of-the-Art Review," *Experimental and Structural Dynamics,* Institute of Sound and Vibration, Southampton.